Measurements of low energy antiparticles with the PAMELA experiment

P. Hofverberg*
for the PAMELA collaboration

*Royal Institute of Technology (KTH)
Stockholm, Sweden,
Email: pth@kth.se

***Abstract*— The PAMELA space telescope was launched on 15th of June 2006. The main goal of the experiment is precision studies of the antiparticle component of the cosmic radiation. Particle rigidity, charge and type can be measured with the three main detectors of the experiment - the silicon tracker, the time-of-flight (ToF) system, and the electromagnetic calorimeter. PAMELA is housed on a Russian Resurs-DK1 satellite which orbits the earth with an inclination of 69 degrees and is therefore exposed to regions with low geomagnetic cutoff, making the detection of low energy antiparticles feasible. The combination of the ToF and silicon tracker allows the antiproton component to be mass-resolved below 1 GV/c, while the electromagnetic calorimeter is used in addition to this above 1 GV/c. The selection of antiprotons below 2 GeV/c is discussed in this paper.**

I. Introduction

The PAMELA experiment [1] is the main piece of scientific equipment on-board the Resurs DK1 satellite which was launched on the 15th of June 2006 from the Baikonour Cosmodrome. The satellite has since been in orbit, and the expected lifetime is at least 3 years, limited by the drag from the residual atmosphere and the solar wind. PAMELA is housed in a pressurized container filled with nitrogen kept at 1 atmosphere pressure. The satellite is travelling in a semi-polar orbit (69°) at an altitude between 350 km and 600 km when passing the north and south pole respectively. The orbital period is about 90 minutes. The trajectory will thus go through regions with varying geomagnetic cutoff. The trajectory also pass the outer electron belt and the South Atlantic Anomaly (SAA).

The PAMELA instrument is measuring the charged component of the cosmic radiation, with a particular emphasis on antiparticles. The measured energy range of antiparticles is the most extended to date, and the statistics at high energy is significantly increased compared to previous experiments. Previous results from PAMELA regarding antiparticles can be found at [2] [3].

PAMELA consists of a number of sub-detectors as illustrated in Figure 1. The core of the PAMELA instrument is the magnetic spectrometer which measures particle rigidity by means of the bending (deflection) of a particle trajectory in a magnetic field, generated by a permanent magnet. A ToF system is employed to provide a trigger for the experiment and is composed of three planes of scintillator, referred to as S1, S2 and S3. This system also provides albedo particle rejection, and a measurement of particle velocity at low energy. Both the ToF system and the spectrometer measure the ionization energy in the detecting layers. This allows for an accurate determination of the absolute charge, and for the separation between antiprotons and electrons below 1 GV/c. An electromagnetic calorimeter is located below the spectrometer. The main task of this device is to separate hadrons and leptons by means of their interaction pattern when traversing the orthogonal layers of absorber and silicon detectors inside the detector. The spatial development of a shower is reconstructed by the layers of silicon detectors which are divided into strips in alternating directions for each plane.

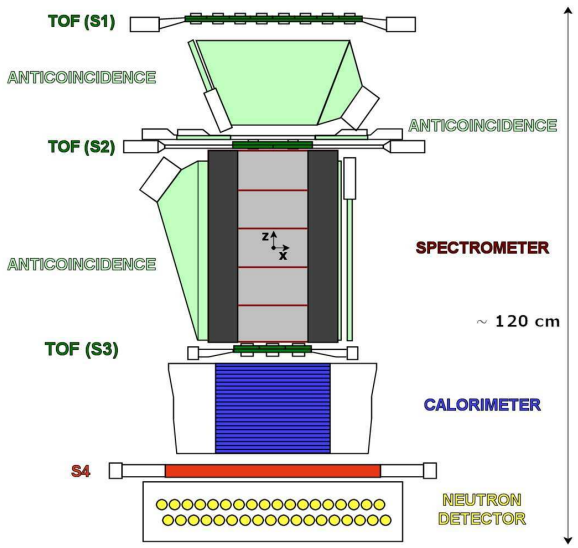

Fig. 1. The PAMELA instrument [9].

A tail-catcher (S4) and a neutron detector is mounted below the calorimeter. These detectors enhance the lepton-hadron separation capability of the calorimeter. The tail-catcher is composed of layers of scintillators read out by photomultipliers.

Surrounding the magnet and on top of it are the first two sets of scintillators, CAS and CAT respectively, that form

the anticoincidence detector. The third (CARD) surrounds the open cavity between S1 and S2. These detectors are used to discriminate against events that do not enter the acceptance cleanly. This could for example happen if a particle enters the experiment through the magnet, interacts, and produces secondaries that give a trigger. The anticoincidence system is made of single sheets of plastic scintillators read out by redundant photomultipliers.

II. Event selection

To select down-going single particle events the following selection was applied: 1) a single track reconstructed by the magnetic spectrometer, fully contained inside the geometrical acceptance and fulfilling the tracker quality selection, defined below, 2) a downward-going particle measured by the Time-of-Flight system, 3) at-least one hit in S1 and S2, consistent with an extra-polated track from the spectrometer, 5) no activity in either of the CAT or CARD anticoincidence detectors, 6) a consistent dE/dx-signal in the different spectrometer planes, 7) an upper limit on the number of energy deposits close to the reconstructed track.

The tracker quality selection comprises of the two requirements, i) a χ^2 of the track fitting less than $(3.6 + 1.85 \times |\text{deflection}|)^4$, ii) a number of points in the track reconstruction greater than or equal to 4 in the x-z view and 3 in the y-z view.

Applying the event selection ensures a clean sample of downward-going single particles with a reliable rigidity reconstruction. Galactic particles were selected by requiring the reconstructed rigidity to be greater than the Störmer Vertical Cutoff multiplied by a factor of 1.2. This factor was tuned by experimental data to ensure an unambiguous selection of galactic particles.

III. $\bar{\text{P}}$,P identification

The proton and antiproton selection is done with a combination of velocity measurements by the ToF system, dE/dx measurements by the tracker and ToF system and by the interaction pattern in the calorimeter.

Protons and antiprotons are assumed to behave identically inside the tracker and ToF system except for their sign of deflection in the magnetic field and their inelastic interactions. The selection criteria in these detectors were therefore developed from the measured properties of protons and their efficiency for selecting protons and antiprotons are assumed to be identical.

The velocity of a particle depends on mass (m) and rigidity (r) as $\beta = 1/\sqrt{1 + \frac{m^2}{r^2}}$. Antiproton and proton candidates are required to have a β inside a band dependent on rigidity, consistent with that of a proton. This is illustrated in Figure 2. The upper limit on β is stricter than the lower limit to increase the electron and pion rejection.

Single charged particles are selected with dE/dx measurements and is done separately for S1, S2 and the tracker. Events with a dE/dx inside a band defined as a function of rigidity

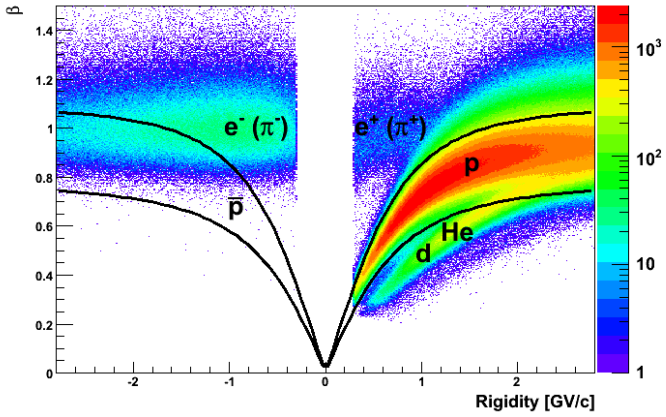

Fig. 2. The β-rigidity distribution for all flight events passing the event selection. Negatively and positively charged particles are assigned a negative and positive rigidity respectively. All particles inside the black lines are selected as (anti)proton candidates.

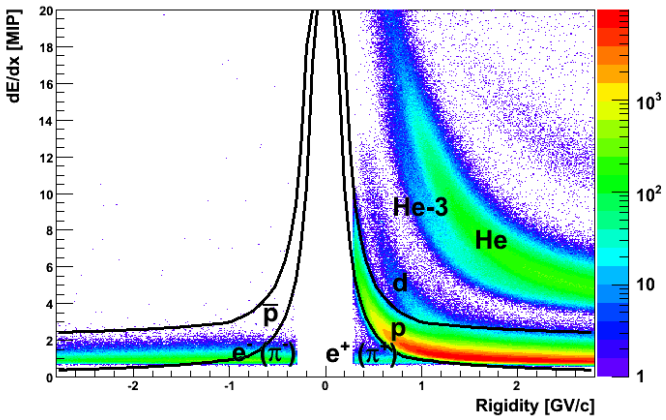

Fig. 3. The dE/dx-rigidity distribution for all flight events passing the event selection. The bands of protons, helium and heavier nuclei are clearly distinguishable. All particles inside the black lines are selected as (anti)proton candidates.

corresponding to single charged particles are selected. The tracker dE/dx selection is illustrated in Figure 3.

The negatively charged events remaining after the velocity and dE/dx selection are made, are antiprotons and predominately electrons. Antiprotons are identified in this sample using the calorimeter. The longitudinal and transverse segmentation of the calorimeter allow hadronic showers to be selected with high efficiency. Antiprotons and protons not interacting in the calorimeter are selected by imposing a cut on the number of strips hit which peaks around 44 for this type of events, together with a requirement of an energy release in the last planes of the calorimeter to reject very inclined electron showers. Late interacting events are selected with a topological variable sensitive to events with a proton-like energy deposit close to the reconstructed track. Interacting events are selected with a cut on the fraction of energy outside a cylinder of radius

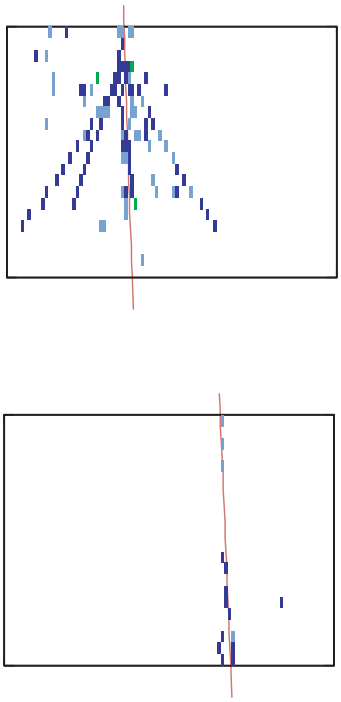

Fig. 4. An interacting (top) and non-interacting (bottom) antiproton inside the calorimeter. The red line corresponds to the track reconstructed by the tracker. The energy deposited in each strip is color coded where light blue corresponds to 0-2 MIP and dark blue to 2-10 MIP.

8 strips. This rejects a large fraction of electrons, which deposit 95 % of their energy inside a cylinder of 7.5 strips, while selecting a substantial part of interacting antiprotons which deposit 95 % of their energy inside a cylinder of radius 10 cm (corresponding to roughly 40 strips). An additional cut is put on the fraction of energy released inside a cylinder of 4 strips. This select events where an antiproton breaks up a nucleus in the detector material and the fragments deposit all their energy in a single strip. A non-interacting and interacting antiproton event is illustrated in Figure 4.

The selection was developed using the PAMELA Collaboration's official simulation program GPAMELA, which is based on the GEANT3 package [10] version 3.21. The simulation reproduces the entire PAMELA apparatus, including the pressure vessel, and has been validated using particle beam data.

The different, and energy dependent, interaction cross-sections for protons and antiprotons in the calorimeter were taken into account by estimating the selection efficiencies for both species. These efficiencies were studied using both simulated protons and antiprotons, and a sample of protons selected from flight data. A scaling factor was calculated from the proton efficiency derived in flight and in simulation, and used to normalize the simulated antiproton efficiency. These efficiencies were used to rescale the number of protons and antiprotons.

IV. Pion and electron contamination

An upper limit on the electron contamination in the selected antiproton sample was estimated by using a combination of simulation and flight data. The rigidity dependent probability of selecting an electron with the antiproton calorimeter selection was obtained from simulations. Convoluting the probability function with the distribution of selected events in flight, before the calorimeter selection is applied, an upper limit on the contamination of electrons is derived. The resultant electron contamination is less than 3 % and decreasing with rigidity.

Pions do not occur naturally in the cosmic radiation but can be created locally in the satellite payload by cosmic ray interactions. A negative pion is indistinguishable from an antiproton above a few GV/c and therefore pose a contamination in the selected antiproton sample. The amount of pion contamination has been estimated using both simulations and experimental data. In the simulations, protons impinging isotropically on PAMELA were generated according to the experimental proton spectrum measured by PAMELA. For the pion production the FLUKA generator [11] was used. The derived pion spectrum below 1 GV/c was compared with the selected pion spectrum from flight data were pions were identified by velocity measurements with the ToF system, dE/dx measurements with the tracker and ToF system, and the calorimeter. The agreement between experimental and simulated data was good. The estimated number of pions remaining after all antiproton selections have been applied is shown in the left column in Table I. The errors are assumed to be Poisson distributed which introduce a systematic error from 0 % to 20 % in the results.

Below 1.2 GV/c, pions are rejected with velocity measurements with the ToF system and the residual pion contamination is zero. Between 1.2 and 2.0 GV/c, the velocity distributions of pions and antiprotons start to merge. The shape of the velocity distribution in this rigidity region can be used to estimate the number of pions in the antiproton sample. By using Kolmogorov-Smirnoff tests on the velocity distribution of the selected antiproton candidates in flight and generated velocity distributions containing $n_{\bar{p}}$ number of antiprotons and $N - n_{\bar{p}}$ number of pions, were N is the number of selected antiproton candidates in flight and $n_{\bar{p}}$ is varied between 0 and N, the pion and antiproton component in the flight sample can be estimated. The result is shown in the right column in Table I. The agreement between simulation and flight in the rigidity interval 0.4 to 2.0 GV/c, where the two methods overlap, is good. The estimated pion contamination is subtracted from the number of selected antiprotons in each bin. Experimental results of the pion contamination are used from 0.4 GV/c to 2 GV/c. At higher rigidities, results from simulations are used.

V. Corrections

The number of selected antiprotons and protons are compensated for i) losses due to hadronic interactions, ii) energy loss in the instrument and iii) charge sign bias of the tracker selection efficiency.

TABLE I

THE CONTAMINATION OF PIONS IN THE ANTIPROTON SAMPLE ESTIMATED WITH SIMULATIONS (LEFT) AND FLIGHT (RIGHT). BOLD FIGURES INDICATE THE NUMBERS THAT ARE SUBTRACTED FROM THE EXPERIMENTAL ANTIPROTON SAMPLE.

Rigidity [GV/c]	N_{π^-} sim.	N_{π^-} flight
0.4-0.8	0	**0**
0.8-1.2	0	**0**
1.2-1.6	6	**6**
1.6-2.0	12	**11**
2.0-2.4	**3**	-
2.4-2.78	**2**	-

Losses due to inelastic collisions in the dome covering the PAMELA acceptance or in the instrument itself were estimated with simulations. Energy loss for protons in the instrument was compensated for using an unfolding method based on Bayes's theorem [5]. Due to the low statistics of antiprotons, a systematic error was instead added to the antiproton spectrum to accommodate for the uncertainties introduced by energy loss. This uncertainty was estimated by simulating a large number of antiproton spectra, identical to the experimentally selected antiproton spectrum, and comparing the spectra on top of the instrument with the spectra in the spectrometer. A final correction (iii) is made to the antiproton spectrum to compensate for the charge sign selection bias that is introduced by the degradation of the tracker. This is estimated with simulations and is shown to be less than 5 %.

VI. CONCLUSION

Methods for selecting protons and antiprotons from the large number of cosmic rays, detected with the PAMELA space experiment, have been discussed. Using ionization, velocity and calorimeter measurements, it has been demonstrated that a sample of antiprotons with a small contamination of electrons can be selected. A non-negligible amount of negative pions are still present in the selected sample. Methods for estimating this contamination has been discussed, and the number of pions in each rigidity bin is derived. Furthermore, corrections to the number of selected antiprotons and protons are discussed.

REFERENCES

[1] P. Picozza et al, Astroparticle Physics, 27, 296, 2007.

[2] O. Adriani et al, *Observation of an anomalous positron abundance in the cosmic radiation*, Subm. to Nature, 2008. arXiv:0810.4995.

[3] O. Adriani et al, *A new measurement of the antiproton-to-proton flux ratio up to 100 GeV in the cosmic radiation*, Subm. to Phys. Rev. Letters, 2008. arXiv:0810.4994.

[4] Y. Asaoka et al, Phys. Rev. Lett.,88, 2002.

[5] G. D'Agostini, NIM, A362, 487-498, 1995.

[6] The Wilcox Solar Observatory, http://wso.stanford.edu/Tilts.html.

[7] I.V. Moskalenko et al, Astrophys. J, 565, 280, 2002.

[8] J.W. Bieber et al, Phys. Rev. Lett., 83, 674-677, 83, 1999.

[9] PAMELA homepage, http://pamela.roma2.infn.it/index.php

[10] R. Brun et al, *Detector description and simulation tool*, CERN program library, 1994.

[11] A. Bruno, Ph.D thesis, University of Bari, 2008.

[12] S. Orito et al, Phys. Rev. Lett.,84, 1078-1081,2000.

[13] K. Abe et al, *Measurement of cosmic-ray low-energy antiproton spectrum with the first BESS-Polar Antartic flight.*, Preprint submitted to Elsevier, 2008.